Quantitative Effects of Coil Packing Density on Cerebral Aneurysm Fluid Dynamics: An *In Vitro* Steady Flow Study

M. Haithem Babiker,[1] L. Fernando Gonzalez,[2] Felipe Albuquerque,[2] Daniel Collins,[3] Arius Elvikis,[3] and David H. Frakes[1,4]

[1]School of Biological and Health Systems Engineering, Arizona State University, 501 E. Tyler, ECG 334, P.O. Box 879709, Tempe, AZ 85287-9709, USA; [2]Barrow Neurological Institute, St. Joseph's Hospital and Medical Center, Phoenix, AZ, USA; [3]Partnership for Research in Spatial Modeling, Arizona State University, Tempe, AZ, USA; and [4]School of Electrical, Computer, and Energy Engineering, Arizona State University, Tempe, AZ, USA

Associate Editor Larry V. McIntire oversaw the review of this article.

Abstract—Over the past 15 years, coil embolization has emerged as an effective treatment option for cerebral aneurysms that is far less invasive than the long-standing convention of surgical clipping. However, aneurysm recurrence after coil embolization is not uncommon: recurrence rates as high as 50% have been reported in the literature. One factor that may contribute to recurrence after coiling is residual flow into the aneurysmal sac. At present, there is limited quantitative knowledge of the relationship between coil packing density and aneurysmal inflow. We present an *in vitro* fluid dynamic study of basilar tip aneurysm models that elucidates this relationship. At physiologically normal flow rates, we found that a packing density of 28.4% decreased aneurysmal inflow by 31.6% in a wide-neck model, and that a packing density of 36.5% decreased aneurysmal inflow by 49.6% in a narrow-neck model. Results also indicated that coiling reduced aneurysmal inflow more significantly at lower parent vessel flow rates, and that coiling reduced neck-plane velocity magnitudes more significantly for narrow-neck aneurysms. Our study provides novel quantitative information that could ultimately contribute to improved outcomes for patients with cerebral aneurysms by enabling more effective coil embolization.

Keywords—PIV, Basilar artery, Embolic coils, Packing density, Cerebral aneurysm.

INTRODUCTION

Subarachnoid hemorrhage (SAH) is a highly lethal condition with a 30-day mortality rate of 45%. SAH affects approximately 33,000 individuals in the United States (US) each year and accounts for up to 5% of all new strokes.[5] An estimated 80% of SAH cases are attributed to ruptured cerebral aneurysms.[20] In total, ruptured cerebral aneurysms cause more than 14,000 SAH fatalities each year in the US alone.[30]

An estimated 2% of adults worldwide live with undiagnosed cerebral aneurysms.[28] When a cerebral aneurysm is diagnosed, it can be treated in several ways. Surgical clipping and coil embolization are two popular options. Surgical clipping, which has been practiced for over 60 years, comprises the placement of a metallic clip across the neck of the aneurysm to immediately exclude the aneurysmal sac from circulation.[4] Endovascular coil embolization is a far less invasive treatment option that was first practiced in the early 1990s.[3,13,26,29] The international subarachnoid aneurysm trial (ISAT), a multicenter randomized trial involving more than 2000 patients, found that surgical treatment was unsuccessful in 31% of cases as opposed to 23% for coil embolization.[23] Furthermore, a nationwide US study reported that, in comparison to surgical clipping, coil embolization resulted in a 23% reduction in hospital charges, a 44% reduction in hospital stay length, and an estimated 50% reduction in mortality rate.[14] Nevertheless, coil embolization is unsuccessful in many cases. Intra-procedure mortality rates of nearly 10% have been reported, and for basilar tip aneurysms, recurrence rates as high as 50% have been reported after initial treatment.[24]

The ultimate goal of coil embolization is to exclude the aneurysm from circulation. When successful, coil embolization facilitates vascular remodeling at the neck of the aneurysm, which seals off the aneurysm from the parent vessel over time. Thrombosis in the aneurysmal sac is an important intermediate step of this process, but the pathway to a favorable outcome

Address correspondence to M. Haithem Babiker, School of Biological and Health Systems Engineering, Arizona State University, 501 E. Tyler, ECG 334, P.O. Box 879709, Tempe, AZ 85287-9709, USA. Electronic mail: haithem.babiker@asu.edu

begins with the immediate goal of coil embolization: to eliminate aneurysmal inflow by occluding the aneurysm. When embolization is incomplete, there is residual flow from the parent vessel into the aneurysm, which may be one factor that contributes to recurrence. Accordingly, post-treatment aneurysmal inflow is a highly relevant clinical parameter.

Aneurysmal inflow is evaluated during treatment based on visual inspection of dynamic angiograms. This evaluation serves as the short-term measure of embolic success or failure in the procedure room. When little or no contrast agent can be visualized entering the aneurysm, embolization is considered to be complete. This is a qualitative exercise, however, and embolizations that are classified as complete based on angiographic inspection may correspond to a broad range of aneurysmal inflows. Once a procedure is complete, follow-up examinations may include magnetic resonance and/or conventional angiography, but both modalities are qualitative in this context and lack the capability to quantify aneurysmal inflow.

Quantitative knowledge of the relationship between coil packing density and aneurysmal inflow could mitigate evaluation uncertainty and facilitate more complete embolization. Clinical studies have correlated high packing density with decreased aneurysmal recurrence, but have never quantified the relationship between packing density and aneurysmal inflow.[27,33] Numerous studies have investigated the effects of coil embolization on aneurysmal fluid dynamics *in silico* using computational fluid dynamics (CFD).[6,8,22] However, authors of those studies have reported that coiled aneurysm fluid dynamics are extremely difficult to simulate well because of highly complex post-deployment coil geometries and fluid structure interactions.[8,22]

Experts in the field have also noted the shortcomings of previous experimental work, and have recognized a need for different methods.[34] Specifically, previous experimental studies have been both limited and primarily qualitative.[2,7,12,15,25,31,32] Flow visualization was used qualitatively in several studies to observe post-embolization reductions in aneurysmal inflow.[12,15] Other *ex vivo* and *in vivo* studies have focused on intra-aneurysmal pressure measurements to characterize changes in fluid dynamics after coil deployment.[2,7,25] Sorteberg et al. used pressure and temperature measurements at a single point inside the aneurysm to quantify local flow variations indirectly.[31,32] Jou et al. also quantified fluid dynamic changes indirectly based on the visualization of contrast agent flow with fluoroscopy.[17] Canton et al. used two-dimensional (2D) particle image velocimetry (PIV) as a qualitative tool to visualize redirected flow at the aneurysmal neck after coiling.[7] However, none of these studies measured post-embolization flows directly, nor did they quantify post-embolization fluid dynamics in relation to coil packing density.

We present an *in vitro* steady flow study of the fluid dynamics in coiled cerebral aneurysms that quantifies the relationship between coil packing density and aneurysmal inflow using three-dimensional (3D) stereo PIV. The study investigates a type of aneurysm that is particularly challenging to embolize, the basilar tip aneurysm, through parametric idealized models. This work is the initial phase of an ongoing effort to establish a foundation for understanding coiled aneurysm fluid dynamics through experimentation with parametric idealized and anatomical models under steady and pulsatile flow conditions. Our ultimate goal is to facilitate improved outcomes for patients with cerebral aneurysms. To our knowledge, this study represents the first time that the relationship between coil packing density and aneurysmal inflow has been quantified, or that 3D PIV has been used to image flow in aneurysm models treated with endovascular coils.

METHODS

Idealized computational models comprising basilar artery bifurcations and basilar tip aneurysms were designed in Solidworks (Solidworks, Concord, MA, USA). The models were designed under physician supervision and were based on *in vivo* angiographic images of basilar tip aneurysm anatomies. One such image is shown in Fig. 1a. In each model, the main axis of each outlet vessel was oriented to the main axis of the parent vessel at a 60° angle. Four millimeter diameters were specified for the parent vessel and outlet vessels, and a 4 mm diameter spherical aneurysm was attached at the parent vessel bifurcation. Different aneurysmal neck-plane sizes were achieved by varying the overlap between the spherical aneurysms and the parent vessel bifurcations. Overlaps of 0.5 and 1 mm were specified for narrow-neck and wide-neck models,
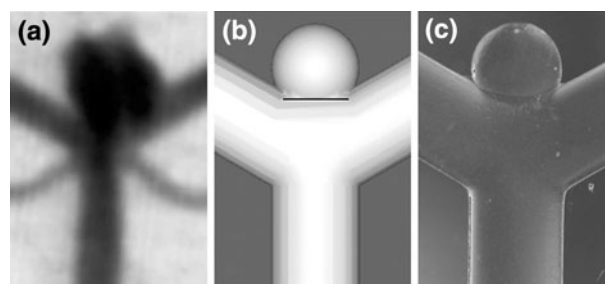

FIGURE 1. *In vivo* angiographic image of basilar tip aneurysm (a), wide-neck computational model with neck-plane indicated in black (b), and wide-neck physical model during experimentation (c).

respectively. These correspond to aneurysmal neck-plane diameters of 2.64 mm (66.0% of the aneurysmal diameter) and 3.46 mm (86.5% of the aneurysmal diameter). The neck-plane represents the boundary that fluid must cross to enter the aneurysm. It is defined here as the smallest circular cross section of the aneurysmal sphere that shares boundaries with the parent vessel. For clarity, we use the term "neck-plane" to refer only to this circular cross section, and not to the entire geometric plane that it resides within. In Fig. 1b, a wide-neck computational model is shown and the projection of the neck-plane onto the model surface is indicated by the black line. In each model, an entrance length of 8 cm (20 vessel diameters) was included upstream of the bifurcation to ensure that flow was fully developed before entering the bifurcation region.

Each computational model was used to construct a physical core model from pot metal with computer numerical controlled (CNC) cutting (Shelley Medical, Toronto, ON, Canada). Transparent physical models were molded around the pot metal cores with Sylgard 184 silicon elastomere (Dow Corning, Midland, MI, USA), and the cores were then melted out. A wide-neck transparent lost-core physical model is shown in Fig. 1c.

The transparent models were connected to a flow loop with flexible polyvinyl chloride tubing. Equal vascular resistances were imposed at each model outlet. A blood analog working fluid composed of water, glycerol, and aqueous sodium iodide was configured to achieve a refractive index of 1.43, matching that of Sylgard 184, and a dynamic viscosity of 3.40 cP at an operating temperature of 25 °C. The working fluid was seeded with 8 μm fluorescent Rhodamine-B particles (Thermo Scientific, Waltham, MA, USA) that experience peak excitation and emission at 542 and 618 nm, respectively. Flow through the loop was driven by a Compuflow 1000 piston pump (Shelley Medical, Toronto, ON, Canada). Data were acquired with a Flowmaster 3D stereo PIV system (Lavision, Ypsilanti, MI, USA). Flow within the models was illuminated by a 0.5 mm thick laser sheet from a 532 nm Solo PIV III dual cavity pulsed YAG laser (New Wave Research, Fremont, CA, USA). Two Imager Intense cross-correlation CCD cameras were used to acquire images with matrix sizes of 1376 by 1040 and pixel dimensions of 9.88 μm square. Low-pass optical filters with a 572 nm cutoff (Omega Optical, Brattleboro, VT, USA) were installed on both cameras. Those filters allowed the fluorescent seed particles to be imaged effectively despite intense laser reflections from deployed coils.

Axium bare platinum detachable coils (EV3, Plymouth, MN, USA) were used to embolize aneurysms within the transparent models. To facilitate deployment, microcatheters were integrated into the flow loop

both upstream and downstream of the model interface. A balloon-assisted technique was used during coil deployment to prevent coil herniation into the parent vessel, as shown in Fig. 2a. Coils were deployed according to standard clinical practice. This was accomplished through the initial deployment of a long coil to create a basket for further coil deployments. Smaller coils were then sequentially deployed to achieve increasing packing densities until no further coils could be deployed without herniation. A clinical "coil pusher" tool was also used after deployment, when necessary, to ensure that the coil mass was oriented internal to the aneurysm and that the aneurysmal neck-plane region could be visualized clearly. Data were acquired after each deployment. An example of a coil packing sequence is shown in Figs. 2b–2d. Coil packing density was calculated analytically and is expressed in our results as the percentage of aneurysmal sac volume occupied by the deployed coils. The coil volumes used in calculation were based upon manufacturer's specifications. Steady flow rates of 3 and 5 mL/s were investigated for each different packing density in both models. These flow rates were chosen to span a physiologic range of normal and diseased conditions.[16] Three planes within the fluid domain were examined for each combination of experimental parameters: the center plane defined by the parent and outlet vessel
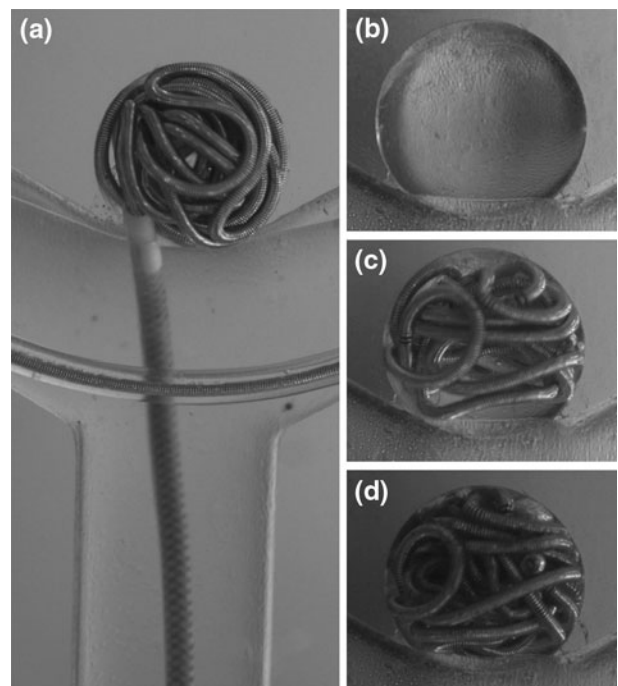

FIGURE 2. Demonstration of balloon-assisted coil deployment technique (a) and progressive stages of a coil deployment sequence in a narrow-neck basilar tip aneurysm model: 0% packing density (b), 19.74% packing density (c), and 28.09% packing density (d).

main axes, and the two planes displaced orthogonally from the center plane by 0.5 mm. At each of these planes, 130 image pairs were acquired at a rate of 5 Hz, with a time separation of 20 μs between images in a pair. Velocity vectors were then calculated through cross-correlation within DaVis software (Lavision, Ypsilanti, MI, USA). Interrogation windows of progressively smaller dimensions were used down to 32 by 32 pixels with a 25% overlap between neighboring windows. Results from each of the 130 image pairs were then averaged to determine a single flow velocity vector field for each plane. RMS errors associated with the averaging process were carefully monitored to ensure that no significant transient flows were present.

The volumes of acquired velocity data were then analyzed to quantify cross-neck flow, defined as the cumulative flow volume crossing the neck-plane of the aneurysm per second, and RMS velocity magnitude at the neck-plane of the aneurysm, calculated as:

$$V_{\mathrm{rms}} = \sqrt{\frac{1}{n}\sum_{i=1}^{n}|V_i|^2}, \qquad (1)$$

where n is the number of data points within the aneurysmal neck-plane and $|V_i|$ indicates the flow velocity magnitude at point i. It is noteworthy that the acquired flow velocity volumes did not span the entire aneurysmal neck-plane in either model configuration, but did span 68.1 and 53.6% of the neck-plane in the narrow and wide-neck models, respectively. Furthermore, each acquired volume was symmetric about the main axes of the parent vessel and outlet vessels, and included the region of the aneurysmal neck-plane toward which the highest magnitude flow velocities were directed from the parent vessel. Accordingly, we are confident that these flow velocity volumes are highly indicative of the overall fluid dynamics at the corresponding neck-planes of the aneurysm models.

For 3D streamtracing and visualization, a modified control grid interpolation (MCGI) was used to reconstruct isotropically resolved 3D velocities throughout the fluid domain spanned by each set of three acquired velocity data planes.[9] MCGI is an established algorithm for fluid flow velocity data reconstruction that performs with high accuracy while minimizing divergence errors.[10] Displacement fields linking similar fluid structures in neighboring velocity magnitude images were determined by minimizing:

$$E(\bar{\alpha}, \bar{\beta}) = \sum_{\mathbf{n} \in R} \sum \big(I[\mathbf{n}, k] - I[n_1 + \bar{\alpha}^T \bar{\theta}(\mathbf{n}), n_2 \\ + \bar{\beta}^T \bar{\phi}(\mathbf{n}), k + \delta k]\big)^2, \qquad (2)$$

where E is the optical flow-based error associated with the displacement field defined by control point row and

column displacements $\bar{\alpha}$ and $\bar{\beta}$, I is an image comprising flow velocity magnitudes, the vector $\mathbf{n} = (n_1, n_2)$ denotes image matrix coordinates, R is the region of support, and $\bar{\theta}$ and $\bar{\phi}$ represent basis functions that implement a bilinear interpolation to populate a complete displacement field based on $\bar{\alpha}$ and $\bar{\beta}$. Sets of displacement fields were then used to facilitate the directional interpolation of individual velocity components, whereby an isotropically resolved volume of 3D flow velocity vectors was reconstructed for each acquired data set. This framework reduces computational requirements in comparison to pure optical flow, at a small expense in terms of displacement field flexibility. More information can be found in the literature.[9–11]

RESULTS

Consistent flow across the neck of the aneurysm was observed in the uncoiled models, as shown in Fig. 3 where vector plots corresponding to different parent vessel flow rates are overlaid on a wide-neck model. In that figure, we have chosen to invert the conventional color map so as to display greater contrast in regions of the vector field characterized by smaller flow velocity magnitudes. Figure 3 also displays the large vortices that formed near the center of the aneurysmal sac in the uncoiled models, which are a common finding in the literature.[12,19,21] After coil deployment, consistent reductions in cross-neck flow were observed. For both models, and for all flow rates examined, increased packing density led to decreased cross-neck flow. As shown in Fig. 4, every incremental increase in packing density was accompanied by a decrease in cross-neck flow. A final packing density of 36.5% in a narrow-neck model led to cross-neck flow decreases of 49.6 and 30.5% for parent vessel flow rates of 3 and 5 mL/s, respectively. A final packing density of 28.4% in a wide-neck model led to cross-neck flow decreases of 31.6 and 27.3% for parent vessel flow rates of 3 and 5 mL/s, respectively. These results can also be appreciated qualitatively in Fig. 5, where several features of the flow field corresponding to the more densely packed aneurysm are consistent with decreased flow across the neck of the aneurysm. Specifically, the cross-neck components of the flow vectors at the neck-plane in Fig. 5b are visibly shorter than those in Fig. 5a (indicating more significant occlusion in Fig. 5b), and the high-velocity jet oriented along the main axis of the parent vessel terminates further upstream in Fig. 5b as compared to Fig. 5a. Another visual representation of the cross-neck flow reduction realized through coiling is provided in Fig. 6, where the respective 3D streamtraces correspond to pre- and post-treatment fluid
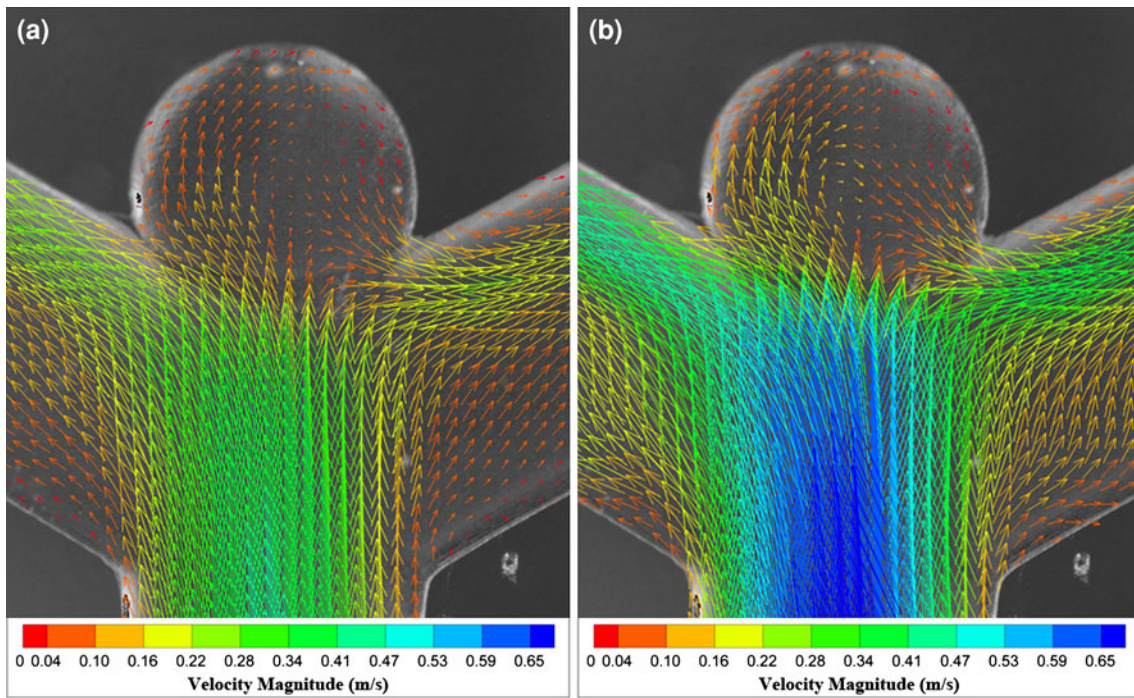
FIGURE 3. Velocity magnitude vectors within the center plane of flow velocity data acquired from an uncoiled wide-neck basilar tip aneurysm model at parent vessel flow rates of 3 (a) and 5 mL/s (b).
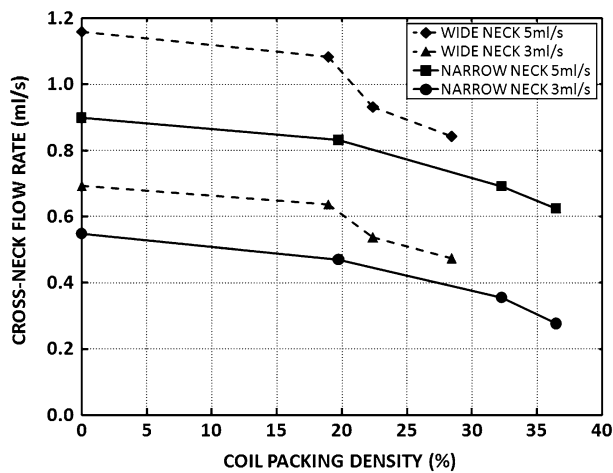

FIGURE 4. Cross-neck flow rate (mL/s) vs. coil packing density (%).

dynamic conditions in a narrow-neck model. In that figure, both sets of streamtraces originate from identical locations within the model center-plane, spread uniformly across the inlet of the bifurcation region.

Similar trends were observed with respect to RMS velocity magnitude at the neck-plane. As shown in Fig. 7, all increases in packing density also led to decreases in RMS velocity magnitude at the neck-plane, with two exceptions. A final packing density of

36.5% in a narrow-neck model led to RMS velocity magnitude decreases of 34.7 and 23.1% for parent vessel flow rates of 3 and 5 mL/s, respectively. A final packing density of 28.4% in a wide-neck model led to RMS velocity magnitude decreases of 7.7 and 16.1% for parent vessel flow rates of 3 and 5 mL/s, respectively. These results can also be appreciated qualitatively in Fig. 5, where the color-coding indicates decreased flow velocity magnitudes at the neck-plane for the more densely packed case. In order to characterize inter-acquisition variations in our results, six repeat data acquisitions were performed for an uncoiled narrow-neck model at a steady parent vessel flow rate of 3 mL/s. Cross-neck flow rates varied from the mean by an average of 4.89% with a standard deviation of 3.31% of the mean. RMS velocity magnitudes at the neck-plane varied from the mean by an average of 3.77% with a standard deviation of 2.43% of the mean.

DISCUSSION AND CONCLUSIONS

The most direct conclusion from our results is that coil embolization significantly reduces both aneurysmal inflow and RMS velocity magnitude at the neck of the aneurysm. However, our results also indicate that even very dense coil packings, by clinical standards, do not embolize completely. In the wide-neck model
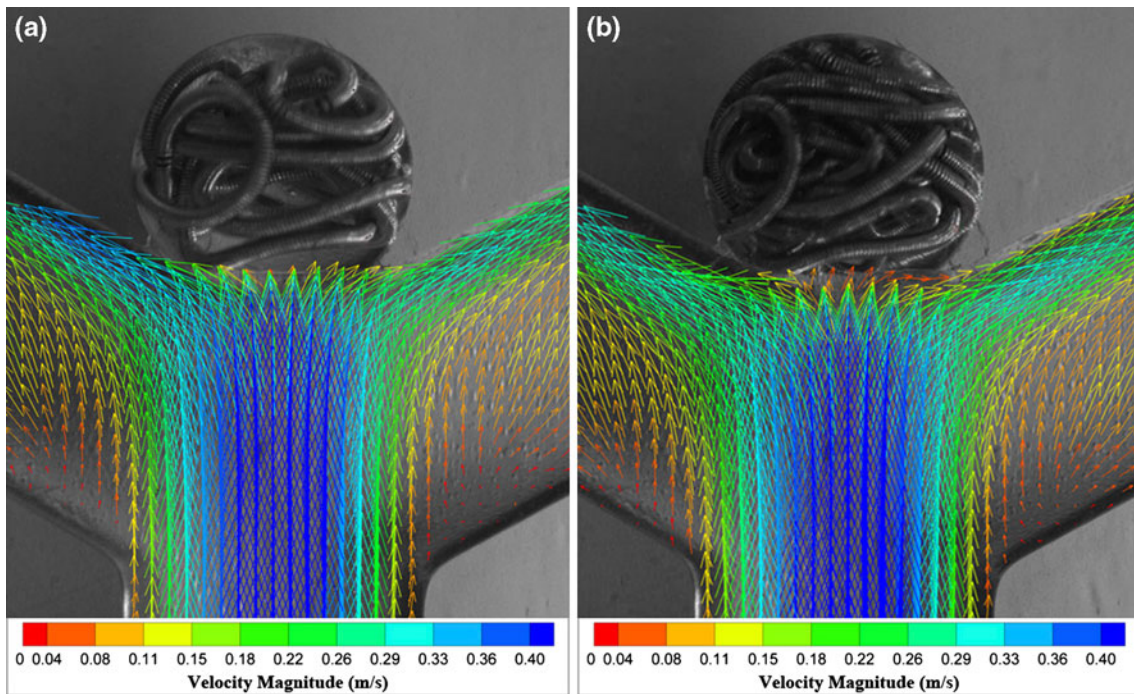
FIGURE 5. Velocity magnitude vectors within the center plane of flow velocity data acquired from a narrow-neck basilar tip aneurysm model at packing densities of 19.74% (a) and 32.27% (b) for a parent vessel flow rate of 3 mL/s.

configuration for example, as much as 72.7% of the cross-neck flow present before coiling persisted at the highest packing density investigated. This suggests that complete embolization, as defined by current clinical evaluation methods, may allow more significant aneurysmal inflow than would be clinically expected.

Two other important conclusions relate specific anatomical and physiologic parameters to post-treatment fluid dynamics. First, our results indicate that coiling reduces aneurysmal inflow more significantly at lower parent vessel flow rates. This finding is consistent with a previous study that evaluated post-treatment aneurysmal inflow.[31] Second, our results indicate that coiling reduces RMS velocity magnitude at the neck-plane more significantly, and more consistently, for narrow-neck aneurysms. We propose that coil embolization may be more effective in establishing a flow stagnation point at the neck-plane for these types of aneurysms, which leads to more significant reductions in flow velocity magnitude at the neck.

Results also showed that the ratio of cross-neck flow reduction to incremental increase in packing density is greater at higher packing densities. Simply put, reductions in aneurysmal inflow per volume unit of coil added were greater for the smaller coils deployed last in the coiling sequence, as compared to the largest coils deployed first. This indicates that deployment of the last coil in a sequence can be very important for achieving acceptably low aneurysmal inflow rates, even

though that coil may change packing density by a small amount. These novel quantitative results support clinical findings that high packing density contributes to decreased aneurysmal recurrence through more complete embolization.[27,33]

There are several ways that quantitative knowledge of the relationship between coil packing density and aneurysmal inflow could facilitate improved outcomes for patients treated with coil embolization. First, neurosurgeons could target an optimal, patient-specific packing density prior to intervention that would limit aneurysmal inflow to an acceptable level. This would encourage the deployment of a sufficient coil volume, if possible, and could reduce the number of procedures resulting in incomplete embolization. A target density would also provide a landmark for neurosurgeons indicating when to stop packing an aneurysm with coils, which would decrease both prolonged anesthesia risks and the risk of aneurysmal rupture due to over-packing.[1] Finally, if a target density could not be achieved in practice, then clinicians would be aware of increased recurrence risk, and could monitor the patient more closely or pursue alternative treatment.

Several limitations of this study are noteworthy. First, because every coil deployment is different, fluid dynamics may vary significantly between two different deployments that achieve the same packing density. Unfortunately, the high cost and limited availability of coils prohibit extensive repeat experimentation. We felt
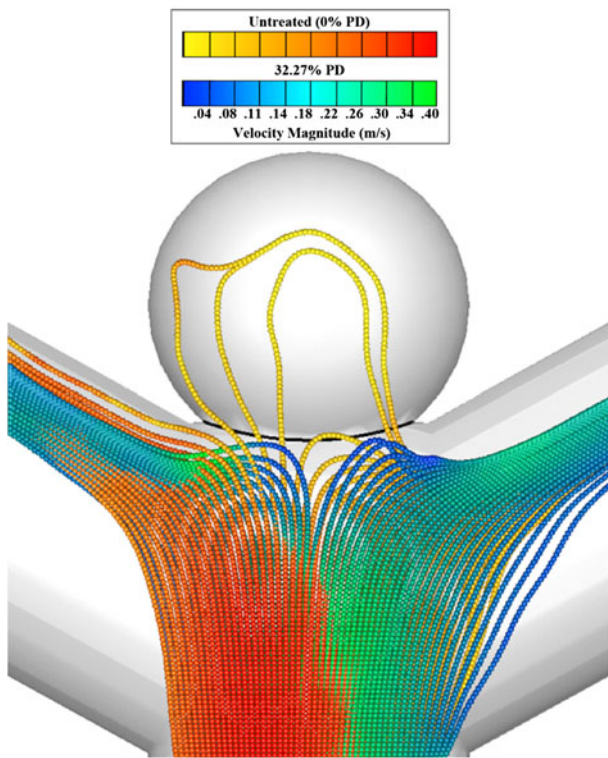
FIGURE 6. Velocity magnitude color-coded 3D streamtraces within reconstructed flow velocity volumes from a narrow-neck basilar tip aneurysm model at 0% packing density (untreated case: *blue/green*) and at 32.27% packing density (treated case: *yellow/red*) for a parent vessel flow rate of 3 mL/s. Both sets of streamtraces originate from identical locations within the model center-plane, spread uniformly across the inlet of the bifurcation region.
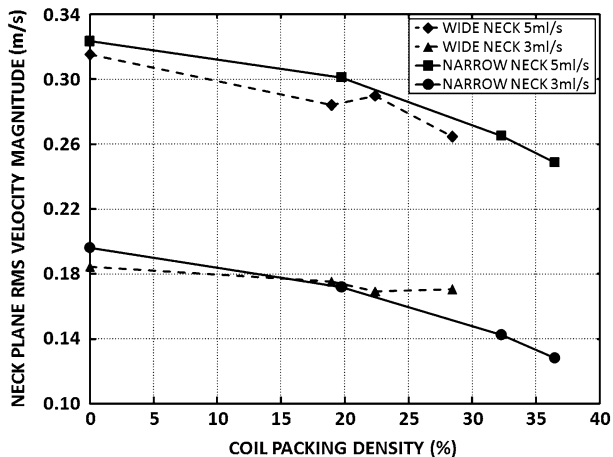

FIGURE 7. Neck-plane RMS velocity magnitude (m/s) vs. coil packing density (%).

that instead of repeating experiments for a few packing densities in one model, our available coil resources would be better used in this initial study by exploring a broad range of packing densities in different models. However, one component of future work will be to

quantify variations in fluid dynamic results among different deployments that achieve the same packing density.

Another limitation of this study is that, within the aneurysmal sac, coils occlude the particles that must be imaged to perform PIV. Accordingly, PIV cannot be used to measure velocities in the aneurysmal sac directly after dense coiling. Instead, we chose to measure velocities at the neck-plane of the aneurysm, which relate directly to intra-aneurysmal fluid dynamics since all flow entering the aneurysmal sac must cross the neck-plane. To avoid any problems with occlusion at the neck-plane, a clinical "coil pusher" tool was used to ensure that coils were sufficiently displaced from the neck-plane to allow for accurate velocity measurements to be taken there with PIV.

This study is also limited in that we explored only idealized models and varied a small number of physiologic and geometric parameters in those models. Physiologically, we focused on models with unregulated compliance under steady flow conditions. Geometrically, we focused on varying aneurysmal neck size and coil packing density, but there are many other geometric parameters that affect flow conditions in coiled aneurysms. For example, previous computational studies have reported that the angle between the main axes of the parent vessel and aneurysm can strongly influence fluid dynamics in basilar tip aneurysms.[18] Clearly, it would be impractical to vary this parameter in a large number of *in vitro* models, which is one disadvantage of bench-top work in comparison to simulation. Furthermore, our study was focused on the instantaneous changes in aneurysmal inflow that induce long-term exclusion of the aneurysmal sac from circulation. The mid- and long-term effects of clotting and other biological processes on aneurysmal fluid dynamics are factors that were not investigated, but need to be considered. Nevertheless, we feel that our data elucidate the effects of varying two important geometric parameters over a physiologic range of steady flow rates spanning normal and diseased conditions. Future work will explore the effects of varying other parameters, and will include both anatomical models and pulsatile flow conditions.

While general trends in risks associated with over-packing and prolonged anesthesia are well-known, specific quantitative risks associated with these factors are less well-known. For this reason, we have considered the impact that our study may have on reducing these risks, but have not tried to quantify that impact as of yet. This quantification is a component of the risk assessment that is one goal of future work.

This study is the initial phase of an ongoing effort to establish a foundation for understanding coiled aneurysm fluid dynamics through *in vitro* experimentation

with PIV. We have quantified the relationship between coil packing density and clinically relevant features of coiled aneurysm fluid dynamics, including cross-neck flow, for parametric idealized basilar tip aneurysm models. Our study provides novel quantitative information that could contribute to improved outcomes for patients with cerebral aneurysms by enabling more effective coil embolization.

ACKNOWLEDGMENTS

REFERENCES

[1]Allen, B. T., C. B. Anderson, B. G. Rubin, R. W. Thompson, M. W. Flye, P. Young-Beyer, P. Frisella, and G. A. Sicard. The influence of anesthetic technique on perioperative complications after carotid endarterectomy. *J. Vasc. Surg.* 19:834–842, 1994.

[2]Boecher-Schwarz, H. G., K. Ringel, L. Kopacz, A. Heimann, and O. Kempski. Ex vivo study of the physical effect of coils on pressure and flow dynamics in experimental aneurysms. *Am. J. Neuroradiol.* 21:1532–1536, 2000.

[3]Brilstra, E., G. Rinkel, Y. V. D. Graaf, W. V. Rooij, and A. Algra. Treatment of intracranial aneurysms by embolization with coils: a systematic review. *Stroke.* 30:470–476, 1999.

[4]Brisman, J., J. Song, and D. Newell. Cerebral aneurysms. *N. Engl. J. Med.* 355:928–939, 2006.

[5]Broderick, J. P., T. Brott, T. Tomsick, R. Miller, and G. Huster. Intracerebral hemorrhage more than twice as common as subarachnoid hemorrhage. *J. Neurosurg.* 78:188–191, 1993.

[6]Byun, H., and K. Rhee. CFD modeling of blood flow following coil embolization of aneurysms. *Med. Eng. Phys.* 26:755–761, 2004.

[7]Canton, G., D. Levy, and J. Lasheras. Changes in the intraaneurysmal pressure due to hydrocoil embolization. *Am. J. Neuroradiol.* 26:904–907, 2005.

[8]Cha, K., E. Balaras, B. Lieber, C. Sadasivan, and A. Wakhloo. Modeling the interaction of coils with the local blood flow after coil embolization of intracranial aneurysms. *J. Biomech. Eng.* 129:873–879, 2007.

[9]Frakes, D., L. Dasi, K. Pekkan, H. Kitajima, K. Sundareswaran, A. Yoganathan, and M. Smith. A new method for registration-based medical image interpolation. *IEEE Trans. Med. Imaging.* 27:370–377, 2008.

[10]Frakes, D., K. Pekkan, L. Dasi, H. Kitajima, D. Zelicourt, H. L. Leo, J. Carberry, K. Sundereswaran, H. Simon, and A. P. Yoganathan. Modified control grid interpolation for the volumetric reconstruction of fluid flows. *Exp. Fluids.* 45:987–997, 2008.

[11]Frakes, D. H., C. P. Conrad, T. M. Healy, J. W. Monaco, M. Fogel, S. Sharma, M. Smith, and A. P. Yoganathan. Application of an adaptive control grid interpolation technique to morphological vascular reconstruction. *IEEE Trans. Biomed. Eng.* 50:197–206, 2003.

[12]Gobin, Y., J. Counord, P. Flaud, and J. Duffaux. In vitro study of haemodynamics in a giant saccular aneurysm model: influence of flow dynamics in the parent vessel and effects of coil embolisation. *Neuroradiology* 36:530–536, 1994.

[13]Hayakawa, M., Y. Murayama, G. R. Duckwiler, Y. P. Gobin, G. Guglielmi, and F. Viñuela. Natural history of the neck remnant of a cerebral aneurysm treated with the Guglielmi detachable coil system. *J. Neurosurg.* 94:561–568, 2000.

[14]Higashida, R., B. J. Lahue, M. T. Torbey, L. N. Hopking, E. Leip, and D. F. Hanley. Treatment of unruptured intracranial aneurysms: a nationwide assessment of effectiveness. *Am. J. Neuroradiol.* 28:146–151, 2007.

[15]Imbesi, S. G., and C. W. Kerber. Analysis of slipstream flow in a wide-necked basilar artery aneurysm: evaluation of potential treatment regimens. *Am. J. Neuroradiol.* 22:721–724, 2001.

[16]Jou, L., A. Mohamed, D. Lee, and M. Mawad. 3D Rotational digital subtraction angiography may underestimate intracranial aneurysms: findings from two basilar aneurysms. *Am. J. Neuroradiol.* 28:1690–1692, 2007.

[17]Jou, L., D. Saloner, and R. Higashida. Determining intraaneurysmal flow for coiled cerebral aneurysms with digital fluoroscopy. *Biomed. Eng. Appl. Basis Commun.* 16:43–48, 2004.

[18]Liou, T., Y. Li, and W. Juan. Numerical and experimental studies on pulsatile flow in aneurysms arising laterally from a curved parent vessel at various angles. *J. Biomech.* 40:1268–1275, 2007.

[19]Mantha, A. R., G. Benndorf, A. Hernandez, and R. W. Metcalfe. Stability of pulsatile blood flow at the ostium of cerebral aneurysms. *J. Biomech.* 42:1081–1087, 2009.

[20]Mayberg, M., H. Batjer, R. Dacey, M. Diringer, E. C. Haley, L. L. Sternau, J. Torner, H. P. Admans, and W. Feinberg. Guidelines for the management of aneurysmal subarachnoid hemorrhage: a statement for healthcare professionals from a special writing group of the Stroke Council, American Heart Association. *Circulation* 90:2592–2605, 1994.

[21]Meckel, S., A. E. Stadler, F. Santini, E. W. Radu, D. A. Rifenacht, M. Markl, and S. G. Wetzel. In vivo visualization and analysis of 3-D hemodynamics in cerebral aneurysms with flow-sensitized 4-D MR imaging at 3 T. *Neuroradiology* 50:473–484, 2008.

[22]Mitsos, A., N. Kakalis, Y. Ventikos, and J. Byrne. Haemodynamic simulation of aneurysm coiling in an anatomically accurate computational fluid dynamics model: technical note. *Neuroradiology* 50:341–347, 2008.

[23]Molyneux, A., R. Kerr, L. Yu, M. Clarke, M. Sneade, J. Yarnold, and P. Sandercock. International subarachnoid aneurysm trial (ISAT) of neurosurgical clipping versus endovascular coiling in 2143 patients with ruptured intracranial aneurysms: a randomised comparison of effects on survival, dependency, seizures, rebleeding, subgroups, and aneurysm occlusion. *Lancet* 366:809–817, 2005.

[24]Murayama, Y., Y. Nien, G. Duckwiler, Y. Gobin, R. Jahan, J. Frazee, N. Martin, and F. Vinuela. Guglielmi

detachable coil embolization of cerebral aneurysms: 11 years' experience. *J. Neurosurg.* 98:959–966, 2003.

[25]Novak, P., R. Glikstein, and G. Mohr. Pulsation–pressure relationship in experimental aneurysms: observation of aneurysmal hysteresis. *Neurol. Res.* 18:377–382, 1996.

[26]Ogilvy, C. S. Neurosurgical clipping versus endovascular coiling of patients with ruptured intracranial aneurysms. *Stroke* 34:2540–2542, 2003.

[27]Raymond, J., F. Guilbert, A. Weill, S. Georganos, L. Juravsky, A. Lambert, J. Lamoureux, M. Chagnon, and D. Roy. Long-term angiographic recurrences after selective endovascular treatment of aneurysms with detachable coils. *Stroke* 34:1398–1403, 2003.

[28]Rinkel, G., M. Djibuti, A. Algra, and J. V. Gijn. Prevalence and risk of rupture of intracranial aneurysms a systematic review. *Stroke* 29:251–256, 1998.

[29]Roy, D., G. Milot, and J. Raymond. Endovascular treatment of unruptured aneurysms. *Stroke* 32:1998–2004, 2001.

[30]Schievink, W. Intracranial aneurysms. *N. Engl. J. Med.* 336:28–40, 1997.

[31]Sorteberg, A., W. Sorteberg, B. Aagaard, A. Rappe, and C. Strother. Hemodynamic versus hydrodynamic effects of Guglielmi detachable coils on intra-aneurysmal pressure and flow at varying pulse rate and systemic pressure. *Am. J. Neuroradiol.* 25:1049–1057, 2004.

[32]Sorteberg, A., W. Sorteberg, A. Rappe, and C. Strother. Effect of Guglielmi detachable coils on intraaneurysmal flow: experimental study in canines. *Am. J. Neuroradiol.* 23:288–294, 2002.

[33]Wakhloo, A., M. Gounis, J. Sandhu, N. Akkawi, A. Schenck, and I. Linfante. Complex-shaped platinum coils for brain aneurysms: higher packing density, improved biomechanical stability, and midterm angiographic outcome. *Am. J. Neuroradiol.* 28:1395–1400, 2007.

[34]Wakhloo, A., B. Lieber, G. Canton, D. Levy, J. Lasheras, and C. Geindreau. Changes of intra-aneurysmal pressure during coiling. *Am. J. Neuroradiol.* 27:471–474, 2006.